Research Article

Utilizing the Updated Gamma-Ray Bursts and Type Ia Supernovae to Constrain the Cardassian Expansion Model and Dark Energy

Jun-Jie Wei,[1,2] Qing-Bo Ma,[1,2] and Xue-Feng Wu[1,3,4]

[1]*Purple Mountain Observatory, Chinese Academy of Sciences, Nanjing 210008, China*
[2]*University of Chinese Academy of Sciences, Beijing 100049, China*
[3]*Chinese Center for Antarctic Astronomy, Nanjing 210008, China*
[4]*Joint Center for Particle, Nuclear Physics and Cosmology, Nanjing University-Purple Mountain Observatory,
 Nanjing 210008, China*

Correspondence should be addressed to Xue-Feng Wu; xfwu@pmo.ac.cn

We update gamma-ray burst (GRB) luminosity relations among certain spectral and light-curve features with 139 GRBs. The distance modulus of 82 GRBs at $z > 1.4$ can be calibrated with the sample at $z \leq 1.4$ by using the cubic spline interpolation method from the Union2.1 Type Ia supernovae (SNe Ia) set. We investigate the joint constraints on the Cardassian expansion model and dark energy with 580 Union2.1 SNe Ia sample ($z < 1.4$) and 82 calibrated GRBs' data ($1.4 < z \leq 8.2$). In ΛCDM, we find that adding 82 high-z GRBs to 580 SNe Ia significantly improves the constraint on $\Omega_m - \Omega_\Lambda$ plane. In the Cardassian expansion model, the best fit is $\Omega_m = 0.24^{+0.15}_{-0.15}$ and $n = 0.16^{+0.30}_{-0.52}$ (1σ), which is consistent with the ΛCDM cosmology ($n = 0$) in the 1σ confidence region. We also discuss two dark energy models in which the equation of state $w(z)$ is parameterized as $w(z) = w_0$ and $w(z) = w_0 + w_1 z/(1+z)$, respectively. Based on our analysis, we see that our universe at higher redshift up to $z = 8.2$ is consistent with the concordance model within 1σ confidence level.

1. Introduction

In recent years, the combined observations of nearby and distant Type Ia supernovae (SNe Ia) have provided strong evidence for the current accelerated expansion of the universe [1–3]. The cause of the acceleration remains unknown. Many authors suggest that the composition of the universe may consist of an extra component called dark energy, which may explain the acceleration of the universe at the current epoch. For example, the dark energy model with a constant equation of state $P/\rho \equiv w = -1$ is one of the several possible explanations for the acceleration, while other models suggest that dark energy changes with time, and there are many ways to characterize the time variation of dark energy. Here, we adopt a simple model in which the dark energy equation of state can be parameterized by $P/\rho \equiv w(z) = w_0 + w_1 z/(1 + z) = w_0 + w_1(1 - a)$ [4, 5], where w_0 is constant, w_1 represents

the time dependence of dark energy, and $a = 1/(1 + z)$ is the scale factor. In addition, models where general relativity is modified can also drive universe acceleration, such as the Cardassian expansion model which is a possible alternative for explaining the acceleration of the universe that invokes no vacuum energy [6].

SNe Ia have been considered a perfect standard candle to measure the geometry and dynamics of the universe. Unfortunately, the farthest SNe Ia detected so far is only at $z = 1.914$ [7]. It is difficult to observe SNe at $z > 2$, even with excellent space-based platforms such as SNAP [8]. And this is quite limiting because much of the most interesting evolution of the universe occurred well before this epoch. Gamma-ray bursts (GRBs) are the most luminous transient events at cosmological distances. Owing to their high luminosities, GRBs can be detected out to very high redshifts [9]. In fact, the farthest burst detected so far is GRB 090423, which is at $z = 8.2$ [10]

(a photometric redshift of 9.4 for GRB 090429B was reported by [11]). Moreover, in contrast to SNe Ia, gamma-ray photons from GRBs are almost immune to dust extinction, so the observed gamma-ray flux is a direct measurement of the prompt emission energy. Hence, GRBs are potentially more promising standard candles than SNe Ia at higher redshifts. The possible use of GRBs as cosmological probes started to become reality after some empirical luminosity relations were discovered. These GRB luminosity relations have been proposed as distance indicators, such as the correlations $\tau_{\mathrm{lag}} - L$ [12], $V - L$ [13], $E_p - E_{\mathrm{iso}}$ [14], $E_p - L$ [15, 16], $E_p - E_\gamma$ [17], and $\tau_{\mathrm{RT}} - L$ [18]. Here the time lag (τ_{lag}) is the time shift between the hard and soft light curves; the luminosity (L) is the isotropic peak luminosity of a GRB; the variability (V) of a burst denotes whether its light curve is spiky or smooth, and V can be obtained by calculating the normalized variance of an observed light curve around a smoothed version of that light curve [13]; (E_p) is the burst frame peak energy in the GRB spectrum; (E_{iso}) is the isotropic equivalent gamma-ray energy; (E_γ) is the collimation-corrected gamma-ray energy; and the minimum rise time (τ_{RT}) in the gamma-ray light curve is the shortest time over which the light curve rises by half of the peak flux of the pulse. However, [19] found that the updated $V - L$ correlation was quite scattered. Its intrinsic scatter has been larger than the one that could be expected of a linear relation.

Generally speaking, with these luminosity indicators, one can make use of them as standard candles for cosmological research. For example, [20] constructed the first GRB Hubble diagram based on nine GRBs using two GRB luminosity indicators. With the $E_p - E_\gamma$ relation, [21] placed tight constraints on cosmological parameters and dark energy. Reference [22] used a model-independent multivariable GRB luminosity indicator to constrain cosmological parameters and the transition redshift. Reference [18] made use of five luminosity indicators calibrated with 69 events by assuming two adopted cosmological models to construct the GRB Hubble diagram. Reference [23] suggested that the time variation of the dark energy is small or zero up to $z \sim 6$ using the $E_p - L$ relation. Reference [24] extended the Hubble diagram up to $z = 5.6$ using 63 gamma-ray bursts (GRBs) via $E_p - L$ relation and found that these GRB data were consistent with the concordance model within 2σ level. In a word, a lot of other works in this so-called GRB cosmology field have been published (please see [19, 25] for reviews). However, there is a so-called circularity problem in the calibration of these luminosity relations. Because of the current poor information on low-z GRBs, these luminosity relations necessarily depend on the assumed cosmology. Some authors attempted to circumvent the circularity problem by using a less model-dependent approach, such as the scatter method [26, 27], the luminosity distance method [28], the Bayesian method [29, 30], and the method by fitting relation parameters of GRBs and cosmological parameters simultaneously [31, 32]. However, these statistical approaches still can not avoid the circularity problem completely, because a particular cosmology model is required in doing the joint fitting. This means that the parameters of the calibrated relations are still coupled to the cosmological parameters derived from a given cosmological model.

To solve the circularity problem completely, one should calibrate the GRB relations in a cosmology-independent way. Recently, a new method to calibrate GRBs in a cosmological model-independent way has been presented [33–35]. This method is very similar to the calibration for SNe Ia by measuring Cepheid variables in the same galaxy, and it is free from the circularity problem. Cepheid variables have been regarded as the first-order standard candles for calibrating SNe Ia which are the secondary standard candles. Similarly, if we regard SNe Ia as the first-order standard candles, we can also calibrate GRBs relations with a large number of SNe Ia since objects at the same redshift should have the same luminosity distance in any cosmology. This method is one of the interpolation procedures which obtain the distance moduli of GRBs in the redshift range of SNe Ia by interpolating from SNe Ia data in the Hubble diagram. Then, if we assume that the GRB luminosity relations do not evolve with redshift, we can extend the calibrated luminosity relations to high-z and derive the distance moduli of high-z GRBs. From these obtained distance moduli, we can constrain the cosmological parameters.

In this paper, we will try to determine the cosmological parameters and dark energy using both the updated 139 GRBs and 580 SNe Ia. In Section 2, we will describe the data we will use and our method of calibration. To avoid any assumption on cosmological models, we will use the distance moduli of 580 SNe Ia from the Union2.1 sample to calibrate five GRB luminosity relations in the redshift range of SNe Ia sample ($z < 1.4$). Then, the distance moduli of 82 high-z GRBs ($z > 1.4$) can be obtained from the five calibrated GRB luminosity relations. The joint constraints on the Cardassian expansion model and dark energy with 580 SNe and 82 calibrated GRBs' data whose $z > 1.4$ will be presented in Section 3. Finally, we will summarize our findings and present a brief discussion.

2. Calibrating the Updated Luminosity Relations of GRBs

2.1. Observational Data and Methodology. As mentioned above, we calibrate the updated luminosity relations of GRBs using low-z events whose distance moduli can be obtained by those of Type Ia supernovae. Actually, we use the cosmology-independent calibration method developed by [33–35]. This method is one of the interpolation procedures which use the abundant SNe Ia sample to interpolate the distance moduli of GRBs in the redshift range of SNe Ia sample ($z < 1.4$). More recently, the Supernova Cosmology Project collaboration released their latest SNe Ia dataset known as the Union2.1 sample, which contains 580 SNe detections [36]. Obviously, there are rich SNe Ia data points, and we can make a better interpolation by using this dataset.

Our updated GRB sample includes 139 GRBs with redshift measurements; there are 57 GRBs at $z < 1.4$ and 82 GRBs at $z > 1.4$. This sample is shown in Table 1, which includes the following information for each GRB: (1) its name; (2) the redshift; (3) the bolometric peak flux P_{bolo}; (4) the bolometric fluence S_{bolo}; (5) the beaming factor f_{beam}; (6) the time lag τ_{lag}; (7) the spectral peak energy E_p; and (8) the minimum rise time τ_{RT}. All of these data were obtained from previously

Table 1: Luminosities and luminosity indicators.

GRB	z	$P_{\rm bolo}$ (erg cm^{-2} s^{-1})	$S_{\rm bolo}$ (erg cm^{-2})	$f_{\rm beam}$	$\tau_{\rm lag}$ (s)	E_p (keV)	$\tau_{\rm RT}$ (s)
970228	0.70	7.30E − 06 ± 4.30E − 07	⋯	⋯	⋯	$115\pm^{38}_{38}$	0.26 ± 0.04
970508	0.84	3.30E − 06 ± 3.30E − 07	8.09E − 06 ± 8.10E − 07	0.0795 ± 0.0204	0.50 ± 0.30	$389\pm^{40}_{40}$	0.71 ± 0.06
970828	0.96	1.00E − 05 ± 1.10E − 06	1.23E − 04 ± 1.20E − 05	0.0053 ± 0.0014	⋯	$298\pm^{30}_{30}$	0.26 ± 0.07
971214	3.42	7.50E − 07 ± 2.40E − 08	⋯	⋯	0.03 ± 0.03	$190\pm^{20}_{20}$	0.05 ± 0.02
980613	1.10	3.00E − 07 ± 8.30E − 08	⋯	⋯	⋯	$92\pm^{42}_{42}$	⋯
980703	0.97	1.20E − 06 ± 3.60E − 08	2.83E − 05 ± 2.90E − 06	0.0184 ± 0.0027	0.40 ± 0.10	$254\pm^{25}_{25}$	3.60 ± 0.50
990123	1.61	1.30E − 05 ± 5.00E − 07	3.11E − 04 ± 3.10E − 05	0.0024 ± 0.0007	0.16 ± 0.03	$604\pm^{60}_{60}$	⋯
990506	1.31	1.10E − 05 ± 1.50E − 07	⋯	⋯	0.04 ± 0.02	$283\pm^{30}_{30}$	0.17 ± 0.03
990510	1.62	3.30E − 06 ± 1.20E − 07	2.85E − 05 ± 2.90E − 06	0.0021 ± 0.0003	0.03 ± 0.01	$126\pm^{10}_{10}$	0.14 ± 0.02
990705	0.84	6.60E − 06 ± 2.60E − 07	1.34E − 04 ± 1.50E − 05	0.0035 ± 0.0010	⋯	$189\pm^{15}_{15}$	0.05 ± 0.02
990712	0.43	3.50E − 06 ± 2.90E − 07	1.19E − 05 ± 6.20E − 07	0.0136 ± 0.0034	⋯	$65\pm^{10}_{10}$	⋯
991208	0.71	2.10E − 05 ± 2.10E − 06	⋯	⋯	⋯	$190\pm^{20}_{20}$	0.32 ± 0.04
991216	1.02	4.10E − 05 ± 3.80E − 07	2.48E − 04 ± 2.50E − 05	0.0030 ± 0.0009	0.03 ± 0.01	$318\pm^{30}_{30}$	0.08 ± 0.02
000131	4.50	7.30E − 07 ± 8.30E − 08	⋯	⋯	⋯	$163\pm^{13}_{13}$	0.12 ± 0.06
000210	0.85	2.00E − 05 ± 2.10E − 06	⋯	⋯	⋯	$408\pm^{14}_{14}$	0.38 ± 0.06
000911	1.06	1.90E − 05 ± 1.90E − 06	⋯	⋯	⋯	$986\pm^{100}_{100}$	0.05 ± 0.02
000926	2.07	2.90E − 06 ± 2.90E − 07	⋯	⋯	⋯	$100\pm^{7}_{7}$	0.05 ± 0.03
010222	1.48	2.30E − 05 ± 7.20E − 07	2.45E − 04 ± 9.10E − 06	0.0014 ± 0.0001	⋯	$309\pm^{12}_{12}$	0.12 ± 0.03
010921	0.45	1.80E − 06 ± 1.60E − 07	⋯	⋯	0.90 ± 0.30	$89\pm^{13.8}_{21.8}$	3.90 ± 0.50
011211	2.14	9.20E − 08 ± 9.30E − 09	9.20E − 06 ± 9.50E − 07	0.0044 ± 0.0011	⋯	$59\pm^{8}_{8}$	⋯
020124	3.20	6.10E − 07 ± 1.00E − 07	1.14E − 05 ± 1.10E − 06	0.0039 ± 0.0010	0.08 ± 0.05	$87\pm^{12}_{18}$	0.25 ± 0.05
020405	0.70	7.40E − 06 ± 3.10E − 07	1.10E − 04 ± 2.10E − 06	0.0060 ± 0.0020	⋯	$364\pm^{90}_{90}$	0.45 ± 0.08
020813	1.25	3.80E − 06 ± 2.60E − 07	1.59E − 04 ± 2.90E − 06	0.0012 ± 0.0003	0.16 ± 0.04	$142\pm^{13}_{14}$	0.82 ± 0.10
020903	0.25	3.40E − 08 ± 8.80E − 09	⋯	⋯	⋯	$2.6\pm^{0.8}_{1.4}$	⋯
021004	2.32	2.30E − 07 ± 5.50E − 08	3.61E − 06 ± 8.60E − 07	0.0109 ± 0.0027	0.60 ± 0.40	$80\pm^{22}_{53}$	0.35 ± 0.15
021211	1.01	2.30E − 06 ± 1.70E − 07	⋯	⋯	0.32 ± 0.04	$46\pm^{6}_{8}$	0.33 ± 0.05
030115	2.50	3.20E − 07 ± 5.10E − 08	⋯	⋯	0.40 ± 0.20	$83\pm^{22}_{53}$	1.47 ± 0.50
030226	1.98	2.60E − 07 ± 4.70E − 08	8.33E − 06 ± 9.80E − 07	0.0034 ± 0.0008	0.30 ± 0.30	$97\pm^{17}_{27}$	0.70 ± 0.20
030323	3.37	1.20E − 07 ± 6.00E − 08	⋯	⋯	⋯	$44\pm^{26}_{90}$	1.00 ± 0.50
030328	1.52	1.60E − 06 ± 1.10E − 07	6.14E − 05 ± 2.40E − 06	0.0020 ± 0.0005	0.20 ± 0.20	$126\pm^{14}_{14}$	⋯
030329	0.17	2.00E − 05 ± 1.00E − 06	2.31E − 04 ± 2.00E − 06	0.0049 ± 0.0009	0.14 ± 0.04	$68\pm^{2.2}_{2.3}$	0.66 ± 0.08
030429	2.66	2.00E − 07 ± 5.40E − 08	1.13E − 06 ± 1.90E − 07	0.0060 ± 0.0029	⋯	$35\pm^{8}_{12}$	0.90 ± 0.20
030528	0.78	1.60E − 07 ± 3.20E − 08	⋯	⋯	12.50 ± 0.50	$32\pm^{5}_{4.7}$	0.77 ± 0.20
040924	0.86	2.60E − 06 ± 2.80E − 07	⋯	⋯	0.30 ± 0.04	$67\pm^{6}_{6}$	0.17 ± 0.02
041006	0.71	2.50E − 06 ± 1.40E − 07	1.75E − 05 ± 1.80E − 06	0.0012 ± 0.0003	⋯	$63\pm^{13}_{13}$	0.65 ± 0.16
050126	1.29	1.10E − 07 ± 1.30E − 08	⋯	⋯	2.10 ± 0.30	$47\pm^{8}_{23}$	3.90 ± 0.80
050318	1.44	5.20E − 07 ± 6.30E − 08	3.46E − 06 ± 3.50E − 07	0.0020 ± 0.0006	⋯	$47\pm^{8}_{15}$	0.38 ± 0.05
050319	3.24	2.30E − 07 ± 3.60E − 08	⋯	⋯	⋯	⋯	0.19 ± 0.04
050401	2.90	2.10E − 06 ± 2.20E − 07	⋯	⋯	0.10 ± 0.06	$118\pm^{18}_{18}$	0.03 ± 0.01
050406	2.44	4.20E − 08 ± 1.10E − 08	⋯	⋯	0.64 ± 0.40	$25\pm^{13}_{35}$	0.50 ± 0.30
050408	1.24	1.10E − 06 ± 2.10E − 07	⋯	⋯	0.25 ± 0.10	⋯	0.25 ± 0.08
050416	0.65	5.30E − 07 ± 8.50E − 08	⋯	⋯	⋯	$15\pm^{2.7}_{2.3}$	0.51 ± 0.30
050502	3.79	4.30E − 07 ± 1.20E − 07	⋯	⋯	0.20 ± 0.20	$93\pm^{35}_{55}$	0.40 ± 0.20
050505	4.27	3.20E − 07 ± 5.40E − 08	6.20E − 06 ± 8.50E − 07	0.0014 ± 0.0007	⋯	$70\pm^{24}_{140}$	0.40 ± 0.15
050525	0.61	5.20E − 06 ± 7.20E − 08	2.59E − 05 ± 1.30E − 06	0.0025 ± 0.0010	0.11 ± 0.02	$81\pm^{1.4}_{1.4}$	0.32 ± 0.03
050603	2.82	9.70E − 06 ± 6.00E − 07	⋯	⋯	0.03 ± 0.03	$344\pm^{52}_{52}$	0.17 ± 0.02
050802	1.71	5.00E − 07 ± 7.30E − 08	⋯	⋯	⋯	⋯	0.80 ± 0.20
050820	2.61	3.30E − 07 ± 5.20E − 08	⋯	⋯	0.70 ± 0.30	$246\pm^{40}_{76}$	2.00 ± 0.50
050824	0.83	9.30E − 08 ± 3.80E − 08	⋯	⋯	⋯	⋯	11.00 ± 2.00
050904	6.29	2.50E − 07 ± 3.50E − 08	2.00E − 05 ± 2.00E − 06	0.0097 ± 0.0024	⋯	$436\pm^{90}_{200}$	0.60 ± 0.20

TABLE 1: Continued.

GRB	z	P_{bolo} (erg cm^{-2} s^{-1})	S_{bolo} (erg cm^{-2})	f_{beam}	τ_{lag} (s)	E_p (keV)	τ_{RT} (s)
050908	3.35	$9.80E - 08 \pm 1.50E - 08$	$\cdots$	$\cdots$	$\cdots$	$41\pm_{9}^{5}$	1.50 ± 0.30
050922	2.20	$2.00E - 06 \pm 7.30E - 08$	$\cdots$	$\cdots$	0.06 ± 0.02	$198\pm_{38}^{22}$	0.13 ± 0.02
051022	0.80	$1.10E - 05 \pm 8.70E - 07$	$3.40E - 04 \pm 1.20E - 05$	0.0029 ± 0.0001	$\cdots$	$510\pm_{22}^{20}$	0.19 ± 0.04
051109	2.35	$7.80E - 07 \pm 9.70E - 08$	$\cdots$	$\cdots$	$\cdots$	$161\pm_{130}^{35}$	1.30 ± 0.40
051111	1.55	$3.90E - 07 \pm 5.80E - 08$	$\cdots$	$\cdots$	1.02 ± 0.10	$\cdots$	3.20 ± 1.00
060108	2.03	$1.10E - 07 \pm 1.10E - 07$	$\cdots$	$\cdots$	$\cdots$	$65\pm_{600}^{10}$	0.40 ± 0.20
060115	3.53	$1.30E - 07 \pm 1.60E - 08$	$\cdots$	$\cdots$	$\cdots$	$62\pm_{19}^{6}$	0.40 ± 0.20
060116	6.60	$2.00E - 07 \pm 1.10E - 07$	$\cdots$	$\cdots$	$\cdots$	$139\pm_{400}^{36}$	1.30 ± 0.50
060124	2.30	$1.10E - 06 \pm 1.20E - 07$	$3.37E - 05 \pm 3.40E - 06$	0.0021 ± 0.0002	0.08 ± 0.04	$237\pm_{76}^{51}$	0.30 ± 0.10
060206	4.05	$4.40E - 07 \pm 1.90E - 08$	$\cdots$	$\cdots$	0.10 ± 0.10	$75\pm_{12}^{12}$	1.25 ± 0.25
060210	3.91	$5.50E - 07 \pm 2.20E - 08$	$1.94E - 05 \pm 1.20E - 06$	0.0005 ± 0.0001	0.13 ± 0.08	$149\pm_{400}^{35}$	0.50 ± 0.20
060223	4.41	$2.10E - 07 \pm 3.70E - 08$	$\cdots$	$\cdots$	0.38 ± 0.10	$71\pm_{100}^{10}$	0.50 ± 0.10
060418	1.49	$1.50E - 06 \pm 5.90E - 08$	$\cdots$	$\cdots$	0.26 ± 0.06	$230\pm_{20}^{20}$	0.32 ± 0.08
060502	1.51	$3.70E - 07 \pm 1.60E - 07$	$\cdots$	$\cdots$	3.50 ± 0.50	$156\pm_{400}^{33}$	3.10 ± 0.30
060510	4.90	$1.00E - 07 \pm 1.70E - 08$	$\cdots$	$\cdots$	$\cdots$	$95\pm_{60}^{30}$	$\cdots$
060526	3.21	$2.40E - 07 \pm 3.30E - 08$	$1.17E - 06 \pm 1.70E - 07$	0.0034 ± 0.0014	0.13 ± 0.03	$25\pm_{5}^{5}$	0.20 ± 0.05
060604	2.68	$9.00E - 08 \pm 1.60E - 08$	$\cdots$	$\cdots$	5.00 ± 1.00	$40\pm_{5}^{5}$	0.60 ± 0.20
060605	3.80	$1.20E - 07 \pm 5.50E - 08$	$\cdots$	$\cdots$	5.00 ± 3.00	$169\pm_{200}^{30}$	2.00 ± 0.50
060607	3.08	$2.70E - 07 \pm 8.10E - 08$	$\cdots$	$\cdots$	2.00 ± 0.50	$120\pm_{190}^{17}$	2.00 ± 0.20
060707	3.43	$1.53E - 07 \pm 2.12E - 08$	$3.41E - 06 \pm 1.96E - 07$	$\cdots$	$\cdots$	$63\pm_{13}^{6}$	$\cdots$
060714	2.71	$2.30E - 07 \pm 1.42E - 08$	$6.88E - 06 \pm 2.47E - 07$	$\cdots$	$\cdots$	$103\pm_{21}^{16}$	$\cdots$
060729	0.54	$1.93E - 07 \pm 1.30E - 08$	$6.43E - 06 \pm 3.16E - 07$	$\cdots$	$\cdots$	$61\pm_{9}^{9}$	$\cdots$
060814	0.84	$1.83E - 06 \pm 4.44E - 08$	$4.94E - 05 \pm 4.91E - 07$	$\cdots$	0.29 ± 0.03	$257\pm_{74}^{35}$	1.65 ± 0.24
060904B	0.70	$4.37E - 07 \pm 2.28E - 08$	$4.05E - 06 \pm 2.17E - 07$	$\cdots$	0.36 ± 0.09	$80\pm_{770}^{12}$	1.00 ± 0.16
060908	2.43	$6.69E - 07 \pm 3.36E - 08$	$7.68E - 06 \pm 1.85E - 07$	$\cdots$	0.26 ± 0.06	$151\pm_{112}^{25}$	0.52 ± 0.09
060926	3.21	$1.56E - 07 \pm 1.22E - 08$	$5.47E - 07 \pm 3.80E - 08$	$\cdots$	1.03 ± 0.11	$20\pm_{11}^{11}$	$\cdots$
060927	5.60	$4.02E - 07 \pm 1.54E - 08$	$2.37E - 06 \pm 8.67E - 08$	$\cdots$	0.12 ± 0.04	$72\pm_{15}^{7}$	0.46 ± 0.12
061007	1.26	$7.20E - 06 \pm 1.11E - 07$	$2.24E - 04 \pm 1.72E - 06$	$\cdots$	0.11 ± 0.01	$399\pm_{12}^{11}$	0.38 ± 0.02
061110A	0.76	$9.79E - 08 \pm 1.35E - 08$	$2.71E - 06 \pm 1.18E - 07$	$\cdots$	$\cdots$	$90\pm_{13}^{13}$	$\cdots$
061110B	3.44	$1.79E - 07 \pm 2.66E - 08$	$6.12E - 06 \pm 3.38E - 07$	$\cdots$	0.24 ± 0.36	$517\pm_{53}^{53}$	0.79 ± 0.64
061121	1.31	$8.04E - 06 \pm 1.07E - 07$	$6.53E - 05 \pm 5.76E - 07$	$\cdots$	0.03 ± 0.01	$606\pm_{55}^{44}$	0.98 ± 0.19
061222B	3.36	$2.29E - 07 \pm 3.15E - 08$	$5.01E - 06 \pm 2.49E - 07$	$\cdots$	$\cdots$	$49\pm_{8}^{8}$	$\cdots$
070110	2.35	$1.12E - 07 \pm 1.36E - 08$	$4.04E - 06 \pm 1.64E - 07$	$\cdots$	$\cdots$	$110\pm_{30}^{30}$	$\cdots$
070208	1.17	$1.39E - 07 \pm 2.06E - 08$	$1.06E - 06 \pm 1.46E - 07$	$\cdots$	$\cdots$	$51\pm_{10}^{10}$	$\cdots$
070318	0.84	$4.10E - 07 \pm 2.12E - 08$	$7.34E - 06 \pm 2.01E - 07$	$\cdots$	$\cdots$	$154\pm_{19}^{19}$	0.72 ± 0.24
070411	2.95	$1.50E - 07 \pm 1.31E - 08$	$6.29E - 06 \pm 2.19E - 07$	$\cdots$	$\cdots$	$83\pm_{11}^{11}$	$\cdots$
070506	2.31	$1.67E - 07 \pm 1.38E - 08$	$5.16E - 07 \pm 3.43E - 08$	$\cdots$	2.52 ± 0.04	$31\pm_{2}^{3}$	0.12 ± 0.06
070508	0.82	$7.67E - 06 \pm 1.18E - 07$	$7.26E - 05 \pm 6.15E - 07$	$\cdots$	0.04 ± 0.01	$233\pm_{7}^{7}$	0.20 ± 0.01
070521	0.55	$2.09E - 06 \pm 5.26E - 08$	$2.97E - 05 \pm 4.00E - 07$	$\cdots$	0.04 ± 0.01	$222\pm_{16}^{12}$	0.58 ± 0.06
070529	2.50	$3.32E - 07 \pm 5.08E - 08$	$7.44E - 06 \pm 4.31E - 07$	$\cdots$	$\cdots$	$180\pm_{52}^{52}$	$\cdots$
070611	2.04	$1.45E - 07 \pm 2.25E - 08$	$9.52E - 07 \pm 8.44E - 08$	$\cdots$	$\cdots$	$92\pm_{30}^{30}$	$\cdots$
070612A	0.62	$2.77E - 07 \pm 4.24E - 08$	$2.72E - 05 \pm 9.37E - 07$	$\cdots$	$\cdots$	$87\pm_{17}^{17}$	2.49 ± 1.48
070714B	0.92	$3.24E - 06 \pm 1.46E - 07$	$8.91E - 06 \pm 6.77E - 07$	$\cdots$	0.03 ± 0.01	$1120\pm_{473}^{230}$	0.45 ± 0.04
070802	2.45	$6.38E - 08 \pm 9.69E - 09$	$6.50E - 07 \pm 7.05E - 08$	$\cdots$	$\cdots$	$70\pm_{25}^{25}$	$\cdots$
070810A	2.17	$2.77E - 07 \pm 1.77E - 08$	$1.59E - 06 \pm 8.43E - 08$	$\cdots$	1.09 ± 0.23	$44\pm_{9}^{9}$	0.73 ± 0.22
071003	1.10	$4.71E - 06 \pm 1.82E - 07$	$6.73E - 05 \pm 1.48E - 06$	$\cdots$	0.38 ± 0.05	$799\pm_{75}^{61}$	0.88 ± 0.07
071010A	0.98	$1.17E - 07 \pm 2.67E - 08$	$4.97E - 07 \pm 6.05E - 08$	$\cdots$	$\cdots$	$27\pm_{10}^{10}$	$\cdots$
071010B	0.95	$9.20E - 07 \pm 2.18E - 08$	$8.37E - 06 \pm 1.16E - 07$	$\cdots$	0.84 ± 0.04	$52\pm_{6}^{8}$	1.21 ± 0.03
071031	2.69	$7.08E - 08 \pm 8.61E - 09$	$2.19E - 06 \pm 1.92E - 07$	$\cdots$	$\cdots$	$24\pm_{7}^{7}$	$\cdots$

TABLE 1: Continued.

GRB	z	P_{bolo} (erg cm^{-2} s^{-1})	S_{bolo} (erg cm^{-2})	f_{beam}	τ_{lag} (s)	E_p (keV)	τ_{RT} (s)
071117	1.33	$2.71E-06 \pm 5.83E-08$	$7.97E-06 \pm 2.02E-07$	$\cdots$	0.60 ± 0.01	$278\pm_{143}^{48}$	0.20 ± 0.02
071122	1.14	$6.76E-08 \pm 2.06E-08$	$1.41E-06 \pm 1.63E-07$	$\cdots$	$\cdots$	$73\pm_{30}^{30}$	$\cdots$
080210	2.64	$2.57E-07 \pm 1.95E-08$	$4.17E-06 \pm 1.41E-07$	$\cdots$	0.53 ± 0.17	$73\pm_{15}^{15}$	0.57 ± 0.44
080310	2.43	$1.83E-07 \pm 1.72E-08$	$5.49E-06 \pm 2.90E-07$	$\cdots$	$\cdots$	$28\pm_{6}^{6}$	0.41 ± 0.55
080319B	0.94	$1.55E-05 \pm 1.91E-07$	$5.25E-04 \pm 3.94E-06$	$\cdots$	0.02 ± 0.01	$651\pm_{8}^{8}$	0.14 ± 0.01
080319C	1.95	$2.22E-06 \pm 7.79E-08$	$1.77E-05 \pm 2.99E-07$	$\cdots$	$\cdots$	$307\pm_{85}^{56}$	0.21 ± 0.12
080330	1.51	$1.33E-07 \pm 1.80E-08$	$8.77E-07 \pm 1.26E-07$	$\cdots$	$\cdots$	$20\pm_{9}^{9}$	$\cdots$
080411	1.03	$1.04E-05 \pm 1.31E-07$	$8.75E-05 \pm 2.01E-07$	$\cdots$	0.21 ± 0.01	$259\pm_{21}^{16}$	0.65 ± 0.01
080413A	2.43	$1.22E-06 \pm 2.65E-08$	$9.86E-06 \pm 1.71E-07$	$\cdots$	0.13 ± 0.03	$170\pm_{48}^{24}$	0.23 ± 0.03
080413B	1.10	$3.17E-06 \pm 8.25E-08$	$8.00E-06 \pm 1.52E-07$	$\cdots$	0.23 ± 0.01	$73\pm_{10}^{10}$	0.50 ± 0.03
080430	0.77	$4.60E-07 \pm 2.15E-08$	$3.01E-06 \pm 1.53E-07$	$\cdots$	0.68 ± 0.08	$80\pm_{15}^{15}$	0.76 ± 0.12
080516	3.20	$2.77E-07 \pm 2.80E-08$	$5.88E-07 \pm 5.50E-08$	$\cdots$	0.15 ± 0.01	$66\pm_{24}^{24}$	$\cdots$
080520	1.55	$8.23E-08 \pm 1.00E-08$	$1.59E-07 \pm 3.00E-08$	$\cdots$	$\cdots$	$12\pm_{5}^{5}$	$\cdots$
080603B	2.69	$7.57E-07 \pm 2.63E-08$	$7.02E-06 \pm 1.78E-07$	$\cdots$	0.08 ± 0.01	$85\pm_{55}^{18}$	0.22 ± 0.03
080605	1.64	$5.99E-06 \pm 1.10E-07$	$4.72E-05 \pm 4.32E-07$	$\cdots$	0.11 ± 0.01	$246\pm_{14}^{11}$	0.22 ± 0.01
080607	3.04	$8.35E-06 \pm 2.42E-07$	$1.00E-04 \pm 0.00E+00$	$\cdots$	0.04 ± 0.01	$394\pm_{35}^{33}$	0.18 ± 0.06
080707	1.23	$1.68E-07 \pm 1.02E-08$	$1.26E-06 \pm 8.87E-08$	$\cdots$	$\cdots$	$73\pm_{20}^{20}$	$\cdots$
080721	2.60	$9.57E-06 \pm 5.01E-07$	$5.99E-05 \pm 3.04E-06$	$\cdots$	0.13 ± 0.05	$485\pm_{41}^{36}$	0.09 ± 0.04
080810	3.35	$9.76E-07 \pm 8.40E-08$	$1.80E-05 \pm 1.30E-06$	$\cdots$	$\cdots$	$313.5\pm_{73.6}^{73.6}$	$\cdots$
080913	6.70	$2.31E-07 \pm 4.00E-08$	$1.15E-06 \pm 1.20E-07$	$\cdots$	$\cdots$	$93.1\pm_{56.1}^{56.1}$	$\cdots$
080916A	0.69	$1.06E-06 \pm 1.60E-07$	$2.19E-05 \pm 7.30E-06$	$\cdots$	$\cdots$	$109\pm_{9}^{9}$	$\cdots$
081121	2.51	$1.87E-06 \pm 4.80E-07$	$1.73E-05 \pm 3.20E-06$	$\cdots$	$\cdots$	$248\pm_{38}^{32}$	$\cdots$
081222	2.77	$2.62E-06 \pm 3.80E-07$	$1.70E-05 \pm 1.40E-06$	$\cdots$	$\cdots$	$134\pm_{9}^{9}$	$\cdots$
090102	1.55	$3.90E-06 \pm 5.60E-07$	$3.66E-05 \pm 3.40E-06$	$\cdots$	$\cdots$	$451\pm_{73}^{58}$	$\cdots$
090323	3.57	$3.80E-06 \pm 6.90E-07$	$1.48E-04 \pm 2.00E-05$	$\cdots$	$\cdots$	$416\pm_{76}^{73}$	$\cdots$
090328	0.74	$7.28E-06 \pm 5.20E-07$	$1.37E-04 \pm 8.00E-06$	$\cdots$	$\cdots$	$653\pm_{45}^{45}$	$\cdots$
090423	8.20	$3.24E-07 \pm 6.80E-08$	$1.17E-06 \pm 3.20E-07$	$\cdots$	$\cdots$	$82\pm_{15}^{15}$	$\cdots$
090424	0.54	$1.80E-05 \pm 1.20E-06$	$5.85E-05 \pm 2.10E-06$	$\cdots$	$\cdots$	$177\pm_{3}^{3}$	$\cdots$
090516	4.11	$5.93E-07 \pm 3.40E-08$	$1.09E-05 \pm 1.60E-06$	$\cdots$	$\cdots$	$185.6\pm_{98.4}^{42.5}$	$\cdots$
090618	0.54	$8.58E-06 \pm 9.60E-07$	$3.39E-04 \pm 2.50E-05$	$\cdots$	$\cdots$	$155.5\pm_{11.1}^{10.5}$	$\cdots$
090715B	3.00	$8.96E-07 \pm 2.49E-07$	$1.09E-05 \pm 1.60E-06$	$\cdots$	$\cdots$	$134\pm_{56}^{30}$	$\cdots$
090812	2.45	$2.17E-06 \pm 2.40E-07$	$3.15E-05 \pm 4.10E-06$	$\cdots$	$\cdots$	$572\pm_{251}^{159}$	$\cdots$
090902B	1.82	$2.72E-05 \pm 3.00E-07$	$3.78E-04 \pm 3.00E-06$	$\cdots$	$\cdots$	$775\pm_{11}^{11}$	$\cdots$
090926	2.11	$1.82E-05 \pm 3.00E-07$	$1.51E-04 \pm 7.70E-06$	$\cdots$	$\cdots$	$314\pm_{4}^{4}$	$\cdots$
090926B	1.24	$5.55E-07 \pm 7.90E-08$	$1.66E-05 \pm 5.00E-07$	$\cdots$	$\cdots$	$78.3\pm_{7}^{7}$	$\cdots$
091018	0.97	$1.82E-06 \pm 8.40E-07$	$4.33E-06 \pm 7.60E-07$	$\cdots$	$\cdots$	$19.2\pm_{18}^{11}$	$\cdots$
091020	1.71	$1.63E-06 \pm 2.00E-07$	$1.68E-05 \pm 3.70E-06$	$\cdots$	$\cdots$	$47.9\pm_{7.1}^{7.1}$	$\cdots$
091029	2.75	$2.82E-07 \pm 1.60E-08$	$5.84E-06 \pm 4.70E-07$	$\cdots$	$\cdots$	$61.4\pm_{17.5}^{17.5}$	$\cdots$
091127	0.49	$4.03E-06 \pm 1.70E-07$	$2.65E-05 \pm 5.00E-07$	$\cdots$	$\cdots$	$36\pm_{2}^{2}$	$\cdots$
091208B	1.06	$3.47E-06 \pm 6.00E-07$	$7.78E-06 \pm 8.80E-07$	$\cdots$	$\cdots$	$124\pm_{20.1}^{19.4}$	$\cdots$

published studies. Before GRB 060607, we take all the data directly from [18]. We adopt the data between GRB 060707 and GRB 080721 from [19]. For those GRBs detected after July 7, 2008, we adopt the data directly from [37]. Applying the interpolation method, we can derive the distance moduli of 57 low-z GRBs and calibrate five GRB luminosity relations with this low-z sample, that is, the $\tau_{\text{lag}} - L$ relation, the $E_p - L$ relation, the $E_p - E_\gamma$ relation, the $\tau_{\text{RT}} - L$ relation, and the $E_p - E_{\text{iso}}$ relation. The isotropic peak luminosity of a burst is calculated by

$$L = 4\pi D_L^2 P_{\text{bolo}}, \tag{1}$$

the isotropic equivalent gamma-ray energy is given by

$$E_{\text{iso}} = 4\pi D_L^2 S_{\text{bolo}} (1 + z)^{-1}, \tag{2}$$

TABLE 2: Best-fitting results.

Relation	a	b	N	r
$\tau_{\text{lag}} - L$	52.32 ± 0.03	-1.10 ± 0.05	27	-0.75
$E_p - L$	52.08 ± 0.02	1.60 ± 0.04	55	0.79
$E_p - E_\gamma$	50.57 ± 0.01	1.76 ± 0.03	12	0.95
$\tau_{\text{RT}} - L$	52.85 ± 0.03	-1.51 ± 0.06	40	-0.66
$E_p - E_{\text{iso}}$	52.81 ± 0.02	1.53 ± 0.04	42	0.73

and the collimation-corrected energy is

$$E_\gamma = E_{\text{iso}} f_{\text{beam}} = 4\pi D_L^2 S_{\text{bolo}} f_{\text{beam}} (1 + z)^{-1}. \quad (3)$$

Here, D_L is the luminosity distance of the burst, P_{bolo} and S_{bolo} are the bolometric peak flux and fluence of gamma-rays, respectively, while $f_{\text{beam}} = (1 - \cos\theta_{\text{jet}})$ is the beaming factor, and θ_{jet} is the jet half-opening angle. We assume each GRB has bipolar jets, and E_γ is the true energy of the bipolar jets.

For convenience, the luminosity relations involved in this paper can be generally written in the power-law forms:

$$\log y = a + b \log x, \quad (4)$$

where a and b are the intercept and slope of the relation, respectively; y is the luminosity (L in units of erg s^{-1}) or energy (E_{iso} or E_γ in units of erg); x is the GRB parameters measured in the rest frame, for example, $\tau_{\text{lag}}(1 + z)^{-1}/(0.1\,\text{s})$, $E_p(1+z)/(300\,\text{keV})$, $E_p(1+z)/(300\,\text{keV})$, $\tau_{\text{RT}}(1 + z)^{-1}/(0.1\,\text{s})$, and $E_p(1 + z)/(300\,\text{keV})$, for the 5 two-variable relations above.

2.2. Calibration. First of all, we obtain the distance moduli of 57 low-z ($z < 1.4$) GRBs by using cubic spline interpolation from the 580 Union2.1 SNe Ia compiled in [36]. The interpolated distance moduli μ of these 57 GRBs and their corresponding errors σ_μ are shown in Figure 1(a). The SNe Ia data are also plotted in Figure 1(a) for comparison. When the cubic spline interpolation is used, the error of the interpolated distance moduli μ for the GRB at redshift z can be calculated by

$$\sigma_\mu = \left[\left(\frac{z_{i+1} - z}{z_{i+1} - z_i} \right)^2 \epsilon_{\mu,i}^2 + \left(\frac{z - z_i}{z_{i+1} - z_i} \right)^2 \epsilon_{\mu,i+1}^2 \right]^{1/2}, \quad (5)$$

where $\epsilon_{\mu,i}$ and $\epsilon_{\mu,i+1}$ are errors of the SNe at nearby redshifts z_i and z_{i+1}, respectively. With D_L in units of Mpc, the predicted distance modulus is defined as

$$\mu = 5 \log (D_L) + 25. \quad (6)$$

Having estimated the distance moduli μ of 57 low-z GRBs in a model-independent way, we can convert μ into luminosity distance D_L by using (6). From (1)–(3) with the corresponding P_{bolo}, S_{bolo}, and f_{beam}, we can calculate L, E_{iso}, and E_γ. In Figures 1(b)–1(f), with the interpolation results, we show the five luminosity indicators for these 57 GRBs at $z < 1.4$. For each relation, we perform a linear least-squares fit, taking into account both the x-axis error and the y-axis error. We also

measure the scatter of each relation with the distance of the data points from the best-fit line, as done by [38]. The best-fitting results of the intercept a and the slope b with their 1σ uncertainties and the linear correlation coefficients for each relation are summarized in Table 2. The best-fitting results derived by using the interpolation method are carried out with these 57 GRBs at $z < 1.4$. In other words, the results are derived by using data from 27, 55, 12, 40, and 42 GRBs for the $\tau_{\text{lag}} - L$, $E_p - L$, $E_p - E_\gamma$, $\tau_{\text{RT}} - L$, and $E_p - E_{\text{iso}}$ relations, respectively.

Reference [19] found no statistically significant evidence for the redshift evolution of the luminosity relations. If the GRB luminosity relations indeed do not evolve with redshift, we can extend the calibrated luminosity relations to high-z ($z > 1.4$) and derive the luminosity (L) or energy (E_{iso} or E_γ) of each burst at high-z by utilizing the calibrated relations. Therefore, the luminosity distance D_L can be derived from (1)–(3). The uncertainty of the value of the luminosity or energy deduced from each relation is

$$\sigma_{\log y}^2 = \sigma_a^2 + \left(\sigma_b^2 \log x\right)^2 + \left(\frac{b}{\ln 10}\frac{\sigma_x}{x}\right)^2 + \sigma_{\text{int}}^2, \quad (7)$$

where σ_a, σ_b, and σ_x are 1σ uncertainties of the intercept a, the slope b, and the GRB measurable parameters x and σ_{int} is the systematic error in the fitting that accounts for the extra scatter of the luminosity relations. Then, we obtain the distance moduli μ for these 82 GRBs at $z > 1.4$ using (6). The propagated uncertainties will depend on whether P_{bolo} or S_{bolo} are given by

$$\sigma_\mu = \left[\left(\frac{5}{2}\sigma_{\log L}\right)^2 + \left(\frac{5}{2\ln 10}\frac{\sigma_{P_{\text{bolo}}}}{P_{\text{bolo}}}\right)^2 \right]^{1/2}, \quad (8)$$

or

$$\sigma_\mu = \left[\left(\frac{5}{2}\sigma_{\log E_{\text{iso}}}\right)^2 + \left(\frac{5}{2\ln 10}\frac{\sigma_{S_{\text{bolo}}}}{S_{\text{bolo}}}\right)^2 \right]^{1/2},$$

$$\sigma_\mu = \left[\left(\frac{5}{2}\sigma_{\log E_\gamma}\right)^2 + \left(\frac{5}{2\ln 10}\frac{\sigma_{S_{\text{bolo}}}}{S_{\text{bolo}}}\right)^2 \right. \quad (9)$$

$$\left. + \left(\frac{5}{2\ln 10}\frac{\sigma_{f_{\text{beam}}}}{f_{\text{beam}}}\right)^2 \right]^{1/2}.$$

Here we ignore the uncertainty of z in our calculations.

After obtaining the distance modulus of each GRB using one of these relations, we use the same method as [18] to calculate the real distance modulus, which is the weighted
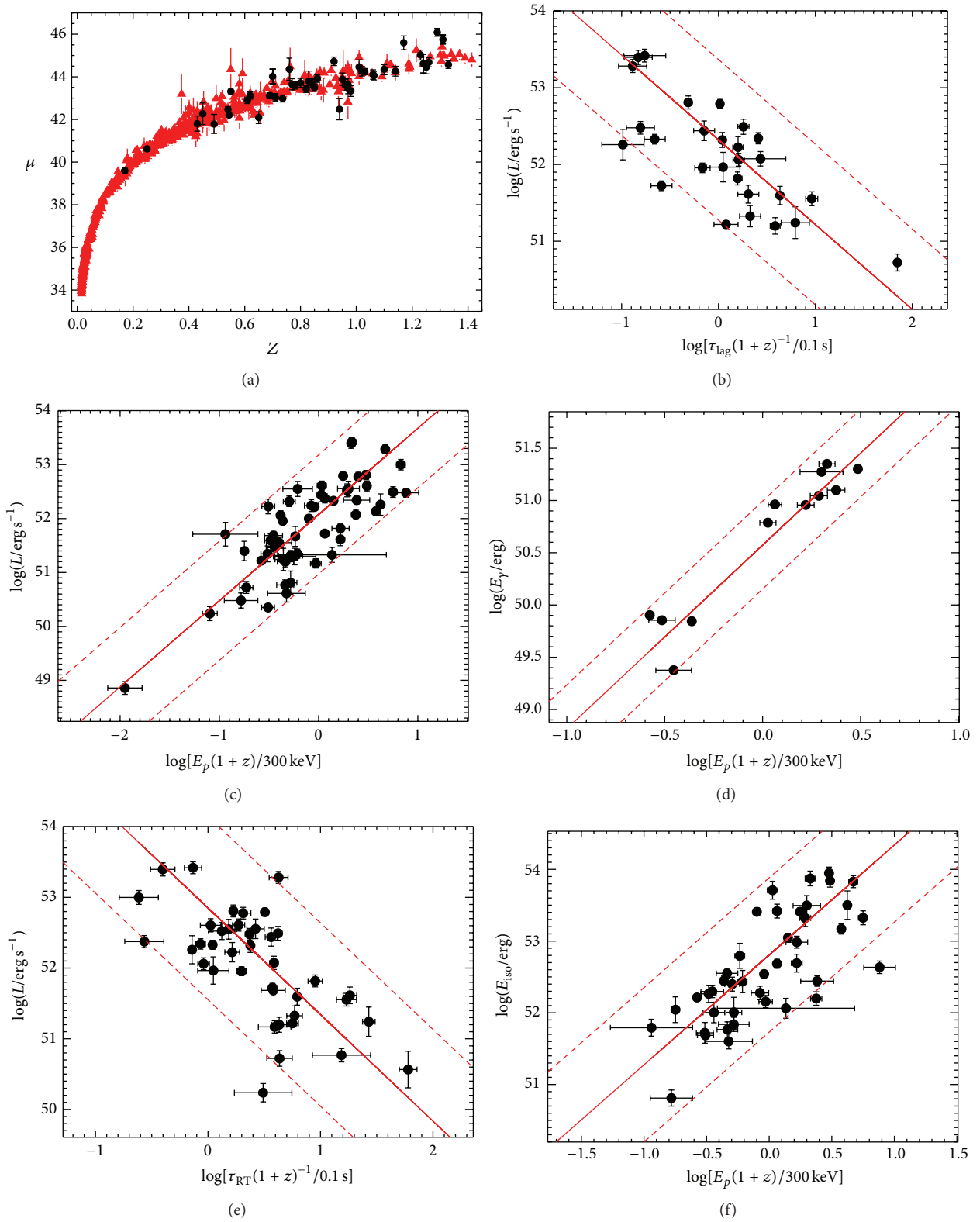
FIGURE 1: (a) The Hubble diagram of 580 SNe Ia (red triangles) and 57 GRBs at $z \leq 1.4$ (black dots) whose distance moduli are derived by using cubic spline interpolation. (b)–(f) The $\tau_{\text{lag}} - L$, $E_p - L$, $E_p - E_\gamma$, $\tau_{\text{RT}} - L$, and $E_p - E_{\text{iso}}$ correlations. The five correlations are calibrated with the sample at $z \leq 1.4$ using cubic spline interpolation. The solid lines show the best-fitting results, while the dashed lines represent their 2σ dispersion around the best fits.
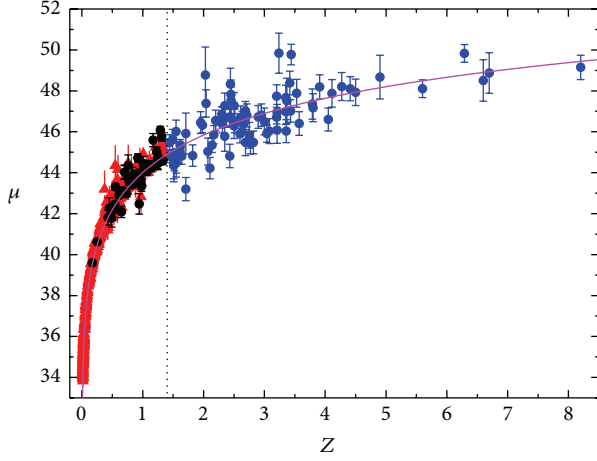
Figure 2: Hubble diagram of 580 SNIa (red triangles) and 139 GRBs (dots) obtained using the interpolation method. The 57 GRBs at $z \leq 1.4$ are obtained by interpolating from SNe Ia data (black dots); and the 82 GRBs at $z > 1.4$ (blue dots) are obtained with the five correlations calibrated with the sample at $z \leq 1.4$ using the cubic spline interpolation method. The vertical dotted line represents $z = 1.4$. The solid curve represents the best-fit cosmology for a flat ΛCDM universe: $\Omega_m = 0.29$, $\Omega_\Lambda = 0.71$.

average of all available distance moduli. The real distance modulus for each burst is

$$\mu_{\text{fit}} = \frac{\sum_i \mu_i / \sigma_{\mu_i}^2}{\sum_i \sigma_{\mu_i}^{-2}}, \tag{10}$$

with its corresponding uncertainty $\sigma_{\mu_{\text{fit}}} = (\sum_i \sigma_{\mu_i}^{-2})^{-1/2}$, where the summation runs from 1 to 5 over the relations with available data and μ_i and σ_{μ_i} are the best estimated distance modulus and its corresponding uncertainty from the ith relation.

Figure 2 shows the Hubble diagram from the Union2.1 SNe Ia sample and 139 GRBs. The combined Hubble diagram is consistent with the concordance cosmology. The 57 GRBs at $z < 1.4$ are obtained using interpolation method directly from SNe data. The 82 GRBs at $z > 1.4$ are obtained by utilizing the five relations calibrated with the sample at $z < 1.4$ using the cubic spline interpolation method.

3. Constraints from Supernovae and GRBs

The latest Type Ia SNe dataset known as the Union2.1 sample was recently released by the Supernova Cosmology Project collaboration, which contains 580 SNe detections (see [36]). With luminosity distance $D_L(\xi, z)$ in units of Mpc (where ξ stands for all the cosmological parameters that define the fitted model), the theoretical distance modulus μ_{th} can be calculated by using (6). The likelihood functions can be determined from the χ^2 statistic:

$$\chi_{\text{SNe}}^2 = \sum_{i=1}^N \frac{[\mu_{\text{th}}(z_i) - \mu_{\text{obs}}(z_i)]^2}{\sigma_{\text{lc}}^2 + \sigma_{\text{ext}}^2 + \sigma_{\text{sample}}^2}, \tag{11}$$

where σ_{lc} is the propagated error from the covariance matrix of the light-curve fit and μ_{obs} is the observational distance modulus. The uncertainties due to host galaxy peculiar velocities, Galactic extinction corrections, and gravitational lensing are included in σ_{ext}, and σ_{sample} is a floating dispersion term containing sample-dependent systematic errors. The confidence regions can be found through marginalizing the likelihood functions over Hubble constant H_0 (i.e., integrating the probability density $p \propto \exp(-\chi^2/2)$ for all values of H_0).

Gamma-ray bursts (GRBs) are the most luminous transient events in the cosmos. Owing to their high luminosity, GRBs can be detected out to the edge of the visible universe, constituting a powerful tool for constructing a Hubble diagram at high-z. We use the above calibration results obtained by using the interpolation methods directly from SNe Ia data. The χ^2 value for the 82 GRBs at $z > 1.4$ is given by

$$\chi_{\text{GRB}}^2 = \sum_{i=1}^N \frac{[\mu_{\text{th}}(z_i) - \mu_{\text{fit},i}]^2}{\sigma_{\mu_{\text{fit},i}}^2}, \tag{12}$$

where $\mu_{\text{fit},i}$ and $\sigma_{\mu_{\text{fit},i}}$ are the fitted distance modulus and its error for each burst. We also marginalize the nuisance parameter H_0.

Motivated by these significant updates in the observations of SNe Ia and GRBs, it is natural to consider the joint constraints on cosmological parameters and dark energy with the latest observational data. We combine SNe Ia and GRBs by multiplying the likelihood functions. The total χ^2 value is

$$\chi_{\text{total}}^2 = \chi_{\text{SNe}}^2 + \chi_{\text{GRB}}^2. \tag{13}$$

The best-fitting values of cosmological model are obtained by minimizing χ_{total}^2.

3.1. ΛCDM Model. In a Friedmann-Robertson-Walker (FRW) cosmology with mass density Ω_m and vacuum energy density Ω_Λ, the luminosity distance is given as

$$D_L(z) = \frac{c}{H_0} \frac{(1+z)}{\sqrt{|\Omega_k|}}$$

$$\cdot \text{sinn} \left\{ |\Omega_k|^{1/2} \int_0^z \frac{dz}{\sqrt{\Omega_m(1+z)^3 + \Omega_\Lambda + \Omega_k(1+z)^2}} \right\}, \tag{14}$$

where c is the speed of light, H_0 is the Hubble constant at the present time, $\Omega_k = 1 - \Omega_m - \Omega_\Lambda$ represents the spatial curvature of the universe, and sinn is sinh when $\Omega_k > 0$ and sin when $\Omega_k < 0$. For a flat universe with $\Omega_k = 0$, (14) simplifies to the form $(1 + z)c/H_0$ times the integral. In this ΛCDM model, the transition redshift satisfies

$$z_T = \left(\frac{2\Omega_\Lambda}{\Omega_m} \right)^{1/3} - 1. \tag{15}$$

We use the datasets discussed above to constrain cosmological parameters. In Figure 3(a), we show the confidence
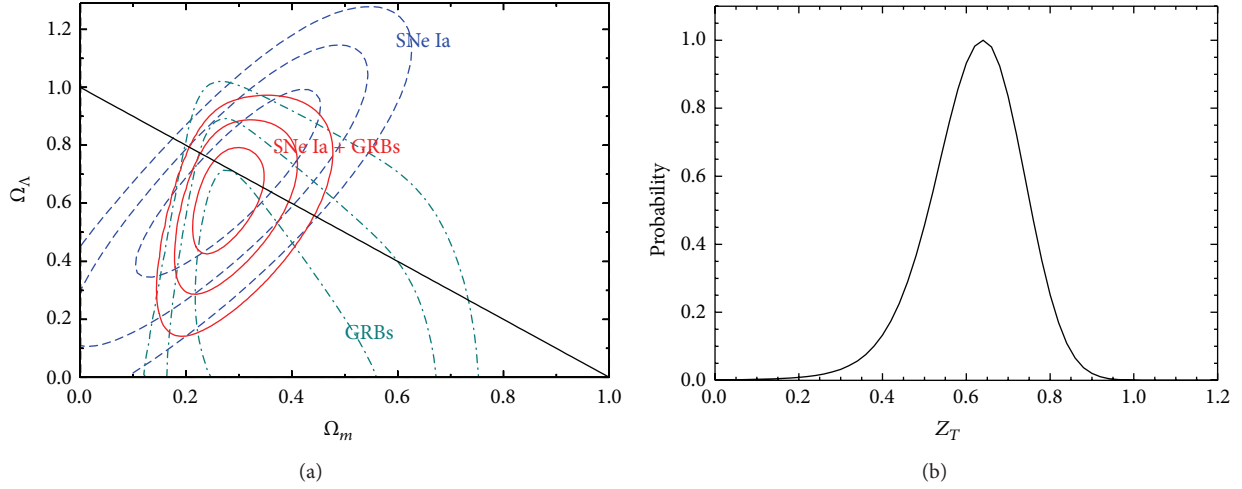
(a)

(b)

FIGURE 3: (a) The contour confidence levels of $(\Omega_m, \Omega_\Lambda)$ in the ΛCDM model from the data for 82 GRBs ($z > 1.4$) (dark cyan dash-dotted lines), 580 SNe Ia (blue dashed lines), and 82 GRBs + 580 SNe Ia (red solid lines), respectively. The contours correspond to 1, 2, and 3σ confidence regions. (b) The probability versus the transition redshift derived from the GRB and SNe Ia sample.

regions for $(\Omega_m, \Omega_\Lambda)$ from 82 GRBs (dark cyan dash-dotted lines), 580 SNe Ia (blue dotted lines), and 82 GRBs + 580 SNe Ia (red solid lines), respectively. We can see that adding 82 high redshift GRBs ($z > 1.4$) to 580 SNe Ia ($z < 1.4$) significantly improves the constraint on $\Omega_m - \Omega_\Lambda$ plane. The 1σ confidence region from all the datasets is $(\Omega_m, \Omega_\Lambda) = (0.27^{+0.08}_{-0.06}, 0.62^{+0.18}_{-0.19})$ with $\chi^2_{\min} = 727.01$ for 659 degrees of freedom. Under the assumption of a flat universe (solid line), the contours yield $(\Omega_m, \Omega_\Lambda) = (0.29^{+0.04}_{-0.04}, 0.71^{+0.04}_{-0.04})$. The transition redshift at which the universe switched from deceleration to acceleration phase is $z_T = 0.64^{+0.08}_{-0.14}$ at the 1σ confidence level (Figure 3(b)).

3.2. Cardassian Expansion Model. Reference [6] proposed the Cardassian expansion model as a possible alternative for explaining the acceleration of the universe that invokes no vacuum energy. This model allows an acceleration in a flat, matter-dominated cosmology. If we consider a spatially flat FRW universe, the Friedmann equation is modified as

$$H^2 = \frac{8\pi G}{3} \left(\rho + C\rho^n \right). \tag{16}$$

This modification may arise as a consequence of embedding our observable universe as a $(3 + 1)$-dimensional brane in extra dimensions or the self-interaction of dark matter. The luminosity distance in this model is given by

$$D_L(z) = cH_0^{-1}(1+z)$$
$$\cdot \int_0^z dz \left[(1+z)^3 \Omega_m + (1 - \Omega_m)(1+z)^{3n} \right]^{-1/2}. \tag{17}$$

Figure 4 shows constraints on Ω_m and n from 1σ to 3σ confidence regions by fitting observational data. The dark cyan dash-dotted lines and blue dashed lines represent the results from 82 GRBs and 580 SNe Ia, respectively. The red
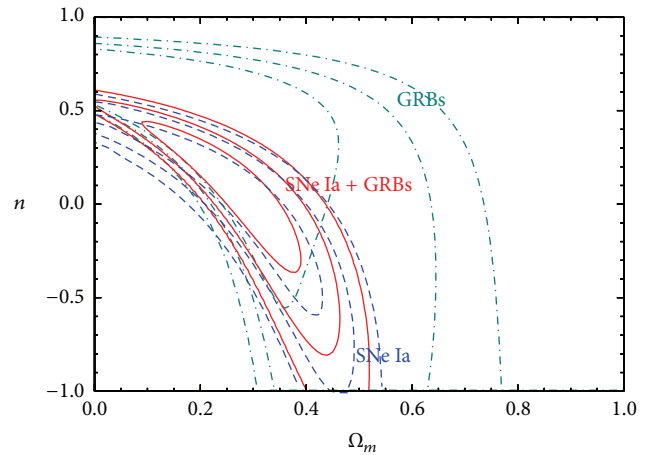

FIGURE 4: The contour confidence levels of (Ω_m, n) in the Cardassian expansion model from the data for 82 GRBs ($z > 1.4$) (dark cyan dash-dotted lines), 580 SNe Ia (blue dashed lines), and 82 GRBs + 580 SNe Ia (red solid lines), respectively. The contours correspond to 1, 2, and 3σ confidence regions.

solid contours show the constraints from the combination of these data. The best values are $\Omega_m = 0.24^{+0.15}_{-0.15}$ and $n = 0.16^{+0.30}_{-0.52}$ at the 1σ confidence level with $\chi^2_{\min} = 727.31$ for 659 degrees of freedom. This result is consistent with the ΛCDM cosmology ($n = 0$) in the 1σ confidence region.

3.3. $w(z) = w_0$ Model: Constant Equation of State. For the dark energy model with a constant equation of state ($w(z) = w_0$), the luminosity distance for a flat universe is [39]

$$D_L(z) = cH_0^{-1}(1+z)$$
$$\cdot \int_0^z dz \left[(1+z)^3 \Omega_m + (1 - \Omega_m)(1+z)^{3(1+w_0)} \right]^{-1/2}, \tag{18}$$
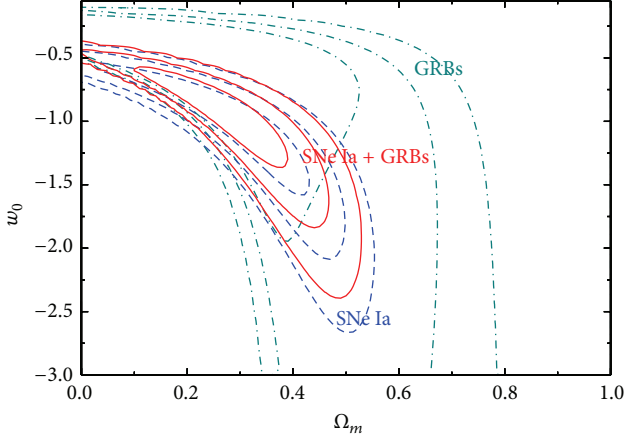
FIGURE 5: Constraints on Ω_m and w_0 from 1σ to 3σ confidence regions with dark energy whose equation state is constant. The contours are derived from GRBs (dark cyan dash-dotted lines), SNe Ia (blue dashed lines), and SNe Ia + GRBs (red solid lines), respectively.

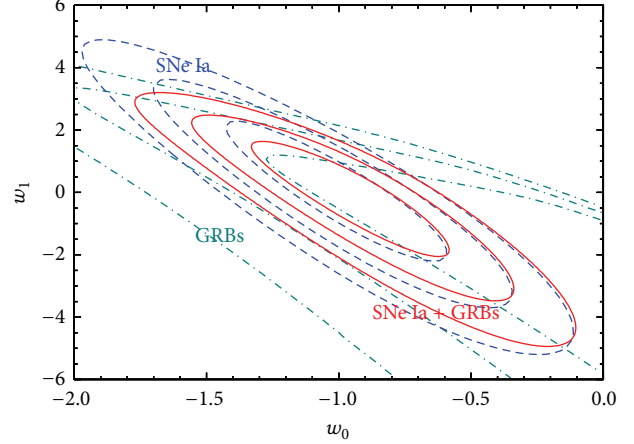
FIGURE 6: Constraints on w_0 and w_1 from 1σ to 3σ confidence regions with dark energy whose equation state is $w(z) = w_0 + w_1 z/(1 + z)$. The contours are derived from GRBs (dark cyan dash-dotted lines), SNe Ia (blue dashed lines), and SNe Ia + GRBs (red solid lines), respectively.

and then the likelihood function depends on Ω_m and w_0. Figure 5 shows the likelihood contours on (Ω_m, w_0) plane for GRBs (dark cyan dash-dotted lines), SNe Ia (blue dashed lines), and SNe Ia + GRBs (red solid lines), respectively. The contours correspond to 1, 2, and 3σ confidence regions, respectively. The cosmological parameters with the largest likelihood are $\Omega_m = 0.24^{+0.16}_{-0.14}$ and $w_0 = -0.85^{+0.28}_{-0.51}$ (1σ) with $\chi^2_{\min} = 727.32$ for 659 degrees of freedom. For a prior of $\Omega_m = 0.29$, we obtain $w_0 = -0.95^{+0.14}_{-0.18}$, which is consistent with the cosmological constant (i.e., $w_0 = -1$) in a 1σ confidence region.

3.4. $w(z) = w_0 + w_1 z/(1 + z)$ Model: Time-Dependent Equation of State. We next examine models in which dark energy changes with time. As shown above, we adopt a simple model in which the dark energy equation of state can be parameterized by [4, 5]

$$w(z) = w_0 + \frac{w_1 z}{(1 + z)}. \tag{19}$$

The ΛCDM model is recovered when $w_0 = -1$ and $w_1 = 0$. In this dark energy model, the luminosity distance is calculated by

$$
\begin{aligned}
D_L(z) = cH_0^{-1}(1 + z) \\
\cdot \int_0^z dz \left[(1 + z)^3 \Omega_m + (1 - \Omega_m) \right. \\
\left. \cdot (1 + z)^{3(1+w_0+w_1)} e^{-3w_1 z/(1+z)} \right]^{-1/2}.
\end{aligned}
\tag{20}
$$

Figure 6 shows the constraints on w_0 versus w_1 from 1σ to 3σ confidence regions. The dark cyan dash-dotted lines and blue dashed lines represent the constraints from 82 GRBs and 580 SNe Ia, respectively. The red solid contours are obtained from the combination of these data. For a prior of $\Omega_m = 0.29$,

we find the best dark energy parameters set is $(w_0, w_1) = (-0.96^{+0.39}_{-0.36}, -0.04^{+1.72}_{-1.96})$ at the 1σ confidence level with $\chi^2_{\min} = 727.54/659$. This result is also consistent with the ΛCDM model (i.e., $w_0 = -1$ and $w_1 = 0$) in the 1σ confidence region.

4. Conclusions and Discussion

In this paper, we have updated five GRB luminosity relations ($\tau_{\text{lag}} - L$, $E_p - E_{\text{iso}}$, $E_p - L$, $E_p - E_\gamma$, and $\tau_{\text{RT}} - L$) among certain spectral and light-curve features with the latest 139 GRBs. We find that the five relations indeed exist with the latest GRBs data. To avoid any assumption on cosmological models, we obtained the distance moduli of 57 low-z ($z < 1.4$) GRBs by using cubic spline interpolation from the 580 Union2.1 SNe Ia compiled in [36]. Then, we calibrated the five relations with these 57 low-z GRBs. In order to constrain cosmological models, we extended the five calibrated luminosity relations to high-z and derived the distance moduli of 82 high-z ($z > 1.4$) GRBs.

Motivated by these significant updates of the observational data, we considered the joint constraints on the Cardassian expansion model and dark energy with 580 Union2.1 SNe Ia sample ($z < 1.4$) and 82 calibrated GRBs' data ($1.4 < z \leq 8.2$). In the ΛCDM cosmology, we find that adding 82 high-z GRBs to 580 SNe Ia significantly improves the constraint on $\Omega_m - \Omega_\Lambda$ plane. We obtain $\Omega_m = 0.27^{+0.08}_{-0.06}$ and $\Omega_\Lambda = 0.62^{+0.18}_{-0.19}$ (1σ). For a flat universe, the contours yield $(\Omega_m, \Omega_\Lambda) = (0.29^{+0.04}_{-0.04}, 0.71^{+0.04}_{-0.04})$. The transition redshift at which the universe switched from deceleration to acceleration phase is $z_T = 0.64^{+0.08}_{-0.14}$ (1σ). In the Cardassian expansion model, we obtain $\Omega_m = 0.24^{+0.15}_{-0.15}$ and $n = 0.16^{+0.30}_{-0.52}$ (1σ). This result is consistent with ΛCDM cosmology ($n = 0$) in the 1σ confidence region, in agreement with the conclusions of [40]. We also fit two dark energy models, including the flat constant w model (i.e.,

$w(z) = w_0$) and the time-dependent w model (i.e., $w(z) = w_0 + w_1 z/(1 + z)$). Based on our analysis, it can be seen that our universe at higher redshift up to $z = 8.2$ is consistent with the concordance model ($\Omega_m = 0.27$, $\Omega_\Lambda = 0.73$, $w_0 = -1$, and $w_1 = 0$) within 1σ level. These results suggest that time dependence of the dark energy is small even if it exists.

Since the discoveries of distance indicators of GRBs, these luminosity indicators have been used as standard candles for cosmological research at high redshifts. However, the dispersion of distance indicators is still large, which restricted the precision of distance measurement by GRBs. The large dispersion may be due to the fact that some contamination of the GRB sample is unavoidable and that pure luminosity indicators may never be found for these sources. Of course, it could also be due to the fact that we simply have not yet identified the correct spectral and light-curve features to use for these luminosity relations. On the other hand, it could also be due to the fact that we are inevitably suffering from the systematic errors and intrinsic scatter associated with the data. In order to estimate distance of GRBs more precisely, we should take efforts to investigate possible origins of dispersion of the distance indicators and/or search for more precise distance indicators in the future.

Conflict of Interests

The authors declare that there is no conflict of interests regarding the publication of this paper.
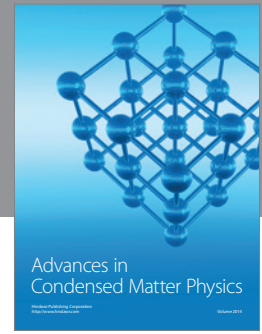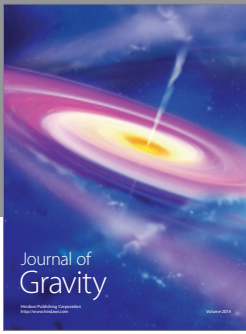
Acknowledgments

References

[1] S. Perlmutter, G. Aldering, M. Della Valle et al., "Discovery of a supernova explosion at half the age of the Universe," *Nature*, vol. 391, no. 6662, pp. 51–54, 1998.

[2] B. P. Schmidt, N. B. Suntzeff, M. M. Phillips et al., "The high-Z supernova search: measuring cosmic deceleration and global curvature of the universe using type IA supernovae," *The Astrophysical Journal*, vol. 507, no. 1, pp. 46–63, 1998.

[3] A. G. Riess, A. V. Filippenko, P. Challis et al., "Observational evidence from supernovae for an accelerating universe and a cosmological constant," *The Astronomical Journal*, vol. 116, no. 3, pp. 1009–1038, 1998.

[4] M. Chevallier and D. Polarski, "Accelerating universes with scaling dark matter," *International Journal of Modern Physics D*, vol. 10, no. 2, pp. 213–223, 2001.

[5] E. V. Linder, "Exploring the expansion history of the universe," *Physical Review Letters*, vol. 90, no. 9, Article ID 091301, 2003.

[6] K. Freese and M. Lewis, "Cardassian expansion: a model in which the universe is flat, matter dominated, and accelerating," *Physics Letters, Section B: Nuclear, Elementary Particle and High-Energy Physics*, vol. 540, no. 1-2, pp. 1–8, 2002.

[7] D. O. Jones, S. A. Rodney, A. G. Riess et al., "The discovery of the most distant known type Ia supernova at redshift 1.914," *The Astrophysical Journal*, vol. 768, no. 2, article 166, 2013.

[8] M. J. Sholl, M. L. Lampton, G. Aldering et al., "SNAP telescope," *Optical, Infrared, and Millimeter Space Telescopes*, vol. 5487, pp. 1473–1483, 2004.

[9] D. Q. Lamb and D. E. Reichart, "Gamma-ray bursts as a probe of the very high redshift universe," *The Astrophysical Journal*, vol. 536, no. 1, pp. 1–18, 2000.

[10] N. R. Tanvir, D. B. Fox, A. J. Levan et al., "A γ-ray burst at a redshift of z≈ 8.2," *Nature*, vol. 461, no. 7268, pp. 1254–1257, 2009.

[11] A. Cucchiara, A. J. Levan, D. B. Fox et al., "A photometric redshift of $z \sim 9.4$ for GRB 090429B," *The Astrophysical Journal*, vol. 736, article 7, 2011.

[12] J. P. Norris, G. F. Marani, and J. T. Bonnell, "Connection between energy-dependent lags and peak luminosity in gamma-ray bursts," *The Astrophysical Journal*, vol. 534, no. 1, pp. 248–257, 2000.

[13] E. E. Fenimore and E. Ramirez-Ruiz, "Redshifts for 220 BATSE gamma-ray bursts determined by variability and the cosmological consequences," http://arxiv.org/abs/astro-ph/0004176.

[14] L. Amati, F. Frontera, M. Tavani et al., "Intrinsic spectra and energetics of BeppoSAX gamma-ray bursts with known redshifts," *Astronomy & Astrophysics*, vol. 390, no. 1, pp. 81–89, 2002.

[15] D. M. Wei and W. H. Gao, "Are there cosmological evolution trends on gamma-ray burst features?" *Monthly Notices of the Royal Astronomical Society*, vol. 345, no. 3, pp. 743–746, 2003.

[16] D. Yonetoku, T. Murakami, T. Nakamura, R. Yamazaki, A. K. Inoue, and K. Ioka, "Gamma-ray burst formation rate inferred from the spectral peak energy-peak luminosity relation," *The Astrophysical Journal*, vol. 609, no. 2, pp. 935–951, 2004.

[17] G. Ghirlanda, G. Ghisellini, and D. Lazzati, "The collimation-corrected gamma-ray burst energies correlate with the peak energy of their νF_ν spectrum," *The Astrophysical Journal*, vol. 616, no. 1, pp. 331–338, 2004.

[18] B. E. Schaefer, "The hubble diagram to redshift >6 from 69 gamma-ray bursts," *The Astrophysical Journal*, vol. 660, no. 1, pp. 16–46, 2007.

[19] F.-Y. Wang, S. Qi, and Z.-G. Dai, "The updated luminosity correlations of gamma-ray bursts and cosmological implications," *Monthly Notices of the Royal Astronomical Society*, vol. 415, no. 4, pp. 3423–3433, 2011.

[20] B. E. Schaefer, "Gamma-ray burst Hubble diagram to z = 4.5," *The Astrophysical Journal Letters*, vol. 583, no. 2, pp. L67–L70, 2003.

[21] Z. G. Dai, E. W. Liang, and D. Xu, "Constraining Ω_M and dark energy with gamma-ray bursts," *The Astrophysical Journal Letters*, vol. 612, no. 2, pp. L101–L104, 2004.

[22] E. Liang and B. Zhang, "Model-independent multivariable gamma-ray burst luminosity indicator and its possible cosmological implications," *The Astrophysical Journal*, vol. 633, no. 2, pp. 611–623, 2005.

[23] Y. Kodama, D. Yonetoku, T. Murakami, S. Tanabe, R. Tsutsui, and T. Nakamura, "Gamma-ray bursts in $1.8 < z < 5.6$ suggest that the time variation of the dark energy is small," *Monthly Notices of the Royal Astronomical Society*, vol. 391, no. 1, pp. L1–L4, 2008.

[24] R. Tsutsui, T. Nakamura, D. Yonetoku et al., "Constraints on ω_0 and ω_a of dark energy from high-redshift gamma-ray bursts," *Monthly Notices of the Royal Astronomical Society: Letters*, vol. 394, no. 1, pp. L31–L35, 2009.

[25] J.-J. Wei, X.-F. Wu, and F. Melia, "The gamma-ray burst hubble diagram and its implications for cosmology," *The Astrophysical Journal*, vol. 772, no. 1, article 43, 2013.

[26] G. Ghirlanda, G. Ghisellini, D. Lazzati, and C. Firmani, "Gamma-ray bursts: new rulers to measure the universe," *The Astrophysical Journal Letters*, vol. 613, no. 1, pp. L13–L16, 2004.

[27] G. Ghirlanda, G. Ghisellini, C. Firmani, L. Nava, F. Tavecchio, and D. Lazzati, "Cosmological constraints with GRBs: homogeneous medium vs. wind density profile," *Astronomy and Astrophysics*, vol. 452, no. 3, pp. 839–844, 2006.

[28] E. Liang and B. Zhang, "Calibration of gamma-ray burst luminosity indicators," *Monthly Notices of the Royal Astronomical Society*, vol. 369, no. 1, pp. L37–L41, 2006.

[29] C. Firmani, G. Ghisellini, G. Ghirlanda, and V. Avila-Reese, "A new method optimized to use gamma-ray bursts as cosmic rulers," *Monthly Notices of the Royal Astronomical Society: Letters*, vol. 360, no. 1, pp. L1–L15, 2005.

[30] F. Y. Wang and Z. G. Dai, "Constraining the cosmological parameters and transition redshift with gamma-ray bursts and supernovae," *Monthly Notices of the Royal Astronomical Society*, vol. 368, no. 1, pp. 371–378, 2006.

[31] L. Amati, C. Guidorzi, F. Frontera et al., "Measuring the cosmological parameters with the $E_{p,i}$–E_{iso} correlation of gamma-ray bursts," *Monthly Notices of the Royal Astronomical Society*, vol. 391, no. 2, pp. 577–584, 2008.

[32] H. Li, M. Su, Z. Fan, Z. Dai, and X. Zhang, "Constraints on dark energy models including gamma ray bursts," *Physics Letters B*, vol. 658, no. 4, pp. 95–100, 2008.

[33] N. Liang, W. K. Xiao, Y. Liu, and S. N. Zhang, "A cosmology-independent calibration of gamma-ray burst luminosity relations and the hubble diagram," *The Astrophysical Journal*, vol. 685, no. 1, pp. 354–360, 2008.

[34] H. Wei and S.-N. Zhang, "Reconstructing the cosmic expansion history up to redshift z=6.29 with the calibrated gamma-ray bursts," *The European Physical Journal C*, vol. 63, no. 1, pp. 139–147, 2009.

[35] H. Wei, "Observational constraints on cosmological models with the updated long gamma-ray bursts," *Journal of Cosmology and Astroparticle Physics*, vol. 2010, no. 8, article 20, 2010.

[36] N. Suzuki, D. Rubin, C. Lidman et al., "The *hubble space telescope* cluster supernova survey. V. Improving the dark-energy constraints above z > 1 and building an early-type-hosted supernova sample," *The Astrophysical Journal*, vol. 746, no. 1, article 85, 2012.

[37] D. Yonetoku, T. Murakami, R. Tsutsui, T. Nakamura, Y. Morihara, and K. Takahashi, "Possible origins of dispersion of the peak energy-brightness correlations of gamma-ray bursts," *Publications of the Astronomical Society of Japan*, vol. 62, no. 6, pp. 1495–1507, 2010.

[38] G. Ghirlanda, G. Ghisellini, C. Firmani, A. Celotti, and Z. Bosnjak, "The peak luminosity-peak energy correlation in gamma-ray bursts," *Monthly Notices of the Royal Astronomical Society*, vol. 360, no. 1, pp. L45–L49, 2005.

[39] A. G. Riess, L.-G. Sirolger, J. Tonry et al., "Type Ia supernova discoveries at $z > 1$ from the *Hubble Space Telescope*: evidence for past deceleration and constraints on dark energy evolution," *The Astrophysical Journal*, vol. 607, no. 2, pp. 665–687, 2004.

[40] C.-J. Feng and X.-Z. Li, "Cardassian universe constrained by latest observations," *Physics Letters B*, vol. 692, no. 2, pp. 152–156, 2010.